

# A portable laser system for high precision atom interferometry experiments

Malte Schmidt<sup>1</sup>, Marco Prevedelli<sup>2</sup>, Antonio Giorgini<sup>3</sup>, Guglielmo M. Tino<sup>3</sup>, Achim Peters<sup>1</sup>

<sup>1</sup> Humboldt-Universität zu Berlin, Institut für Physik, Newtonstraße 15, 12489 Berlin, Germany,  
email: malte.schmidt@physik.hu-berlin.de, Tel. +49-30-2093-4941, Fax. +49-30-2093-4718

<sup>2</sup> Dipartimento di Fisica, Università di Bologna, Via Irnerio 46, 40127 Bologna, Italy

<sup>3</sup> Dipartimento di Fisica e Astronomia and LENS, Università di Firenze-INFN, via Sansone 1 Polo Scientifico, 50019 Sesto Fiorentino (Firenze), Italy

Received: date / Revised version: date

**Abstract** We present a modular rack-mounted laser system for the cooling and manipulation of neutral rubidium atoms which has been developed for a portable gravimeter based on atom interferometry that will be capable of performing high precision gravity measurements directly at sites of geophysical interest. This laser system is constructed in a compact and mobile design so that it can be transported to different locations, yet it still offers improvements over many conventional laboratory-based laser systems. Our system is contained in a standard 19" rack and emits light at five different frequencies simultaneously on up to 12 fibre ports at a total output power of 800 mW. These frequencies can be changed and switched between ports in less than a microsecond. The setup includes two phase-locked diode lasers with a phase noise spectral density of less than  $1 \mu\text{rad}/\text{Hz}^{1/2}$  in the frequency range in which our gravimeter is most sensitive to noise. We characterize this laser system and evaluate the performance limits it imposes on an interferometer.

## 1 Introduction

Since first experimental demonstrations in 1991 [1,2,3,4], atom interferometry has developed into a powerful tool for the ultra precise measurement of accelerations and rotations. It is now used in various laboratories for experiments in the fields of fundamental physics [5,6] and metrology [7,8,9]. In principle, this new technique is also ideally suited for high-accuracy field research such as gravity mapping, geophysics, seismology or navigation [10] and could substantially exceed that of classical gravimeters [11]. However, due to the complexity of these experiments they were so far confined to laboratory environments. Only in recent years efforts have

been undertaken to develop mobile atom interferometers [12,13] that might in future versions also be used on satellite missions [14,15]. Our transportable high-precision gravimeter GAIN (Gravimetric Atom Interferometer) is designed specifically for geophysical on-site measurements.

The working principle of a gravimetric atom interferometer has been described in detail elsewhere [7,16]. In short: An ensemble of laser-cooled neutral atoms (in our case Rubidium 87) is prepared in a 3D Magneto-Optical Trap (MOT), further cooled in optical molasses, and launched upwards. During their parabolic flight, the atoms are subjected to three pulses from counterpropagating laser beams, thereby inducing two-photon Raman transitions that transfer them between the two hyperfine ground states via a stimulated Raman process. The sequence consists of one  $\frac{\pi}{2}$ -, one  $\pi$ -, and finally another  $\frac{\pi}{2}$ -pulse, which constitute an atom optic beam splitter, mirror and recombiner, respectively. Thereby the atomic wave packet is split into two parts that travel on different trajectories due to momentum transfer from the photons. At the output of the atom interferometer the transition probability  $P$  from one hyperfine state to the other is given by  $P = \frac{1}{2}(1 + C \cos \Delta\Phi)$ , where  $\Delta\Phi$  is the accumulated phase difference between wave packets and  $C$  the contrast of the measurement. This includes an acceleration contribution of  $\Delta\Phi_g = k_{\text{eff}} g T^2$  with  $T$  being the time between two consecutive Raman pulses,  $k_{\text{eff}} = k_1 + k_2$  the sum of the two individual counterpropagating Raman laser wavenumbers  $k_i$ , and  $g$  the local gravitational acceleration.

In this paper, we describe in detail the realization of the atomic gravimeter's laser system and characterize its subcomponents. The sensor's physics package (i.e. main chamber and attached optics and electronics, vibration isolation system, control system), first high-precision gravity measurements as well as the instrument's perfor-

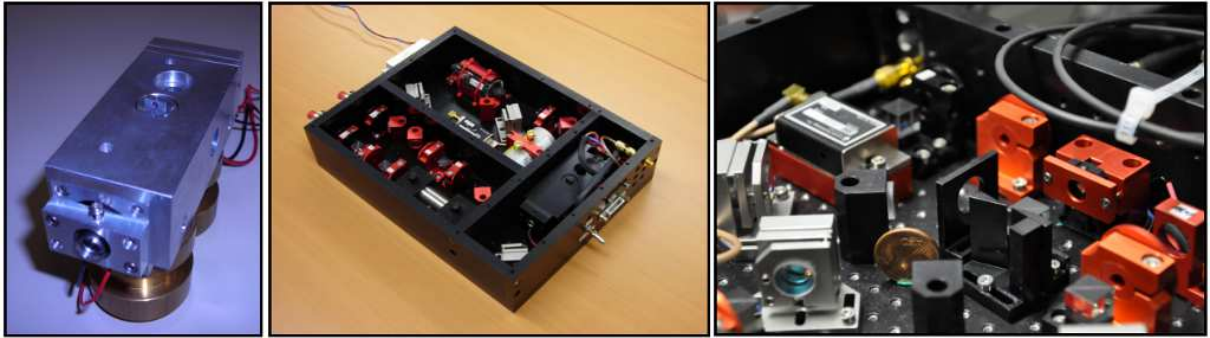


**Fig. 1** Custom-made miniaturized optical mounts. Beam height for all optics is 20 mm, round optical components have a diameter of 0.5". Left to right: External Cavity Diode Laser, Reference laser module, Raman laser module detail with a 5-Eurocent coin ( $d = 21$  mm) as reference

mance in the field will be discussed in future publications.

## 2 Concept

Naturally, the laser system for a mobile atom interferometer has to be mobile and compact as well. Our system is designed to be “truckable” (i.e. easily transportable by a small truck from one gravity measurement site to the next), requiring a rethermalization and readjustment time of less than a day. It will operate at gravimetry reference points where the absolute gravity value is measured in regular intervals [17]. These points are usually selected to be inside of buildings with an environment that is relatively stable, as conventional gravimeters are sensitive to changes in their operating environment (although harsher conditions can be found at more unusual measurement sites). We can thus expect to typically encounter environments with temperature variations of one or two Kelvin, low vibrational noise level and no direct sun light. This is, however, still considerably worse than conditions usually found in laboratory cold atom experiments. Standard laser systems for these experiments are not only quite complex, but also can rarely endure significant mechanical vibrations, thermal fluctuations of even a few Kelvin or electromagnetic noise, without losing laser frequency locks or a significant decrease in optical power output.

A first step in solving these problems was the redesign from scratch of almost all optical mounts, as standard laboratory equipment rarely offers sufficient mechanical stability and is in most cases simply too large for our purposes (Figure 1). Many of these mount designs are adapted from the QUANTUS drop tower project [18] and have proven their stability even under extreme accelerations of up to  $50 g$ . We have mounted all optics in four closed, compact modules with 1 cm thick walls and a beam height of 20 mm for high ruggedness. Light is transferred between the modules by means of polarisation maintaining optical fibres. Except for the reference laser, which is even smaller, each module’s base area is

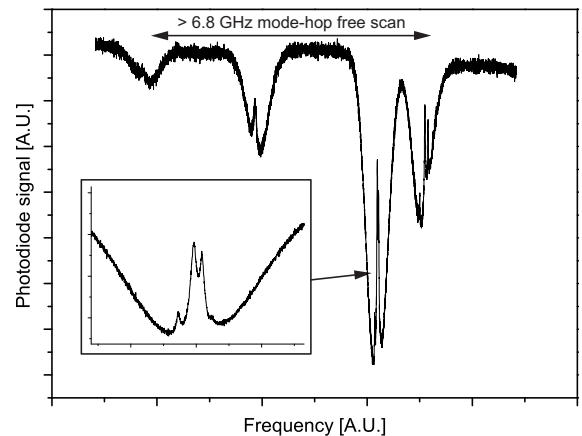


**Fig. 2** Mode-hop free scan over the complete  $^{87}\text{Rb}$  D2 line spectrum using one of our ECDLs. Insert:  $^{85}\text{Rb}$   $F=3 \rightarrow F'$  lines that we use to stabilise the laser.

42 by 42 cm with a height of a few centimeters. The base plate of two of these modules is a custom made Thorlabs aluminium honeycomb breadboard with a 1 cm grid of M3 threads which provides stability as well as flexibility for possible future modifications. The other two modules use 25 mm thick aluminum slabs as base plates with the four walls and two additional divider walls mounted in a force-fit such that under mechanical stress the assembled modules behave as if manufactured from one piece. Fibre and electrical connections are mounted on the walls of each module, the total height of each module varies between 75 and 105 mm.

As laser sources we have built compact external cavity diode lasers (ECDL) that have been adapted from a design developed at SYRTE [19] using Sharp GH0781-JA2C laser diodes. They include an interference filter as a wavelength selector that is one order of magnitude less sensitive to angular misadjustments than gratings found in conventional ECDL configurations which makes it suitable for our application. The output power is up to 50 mW and the intrinsic linewidth less than 10 kHz. The cavity length is 80 mm which gives a free spectral

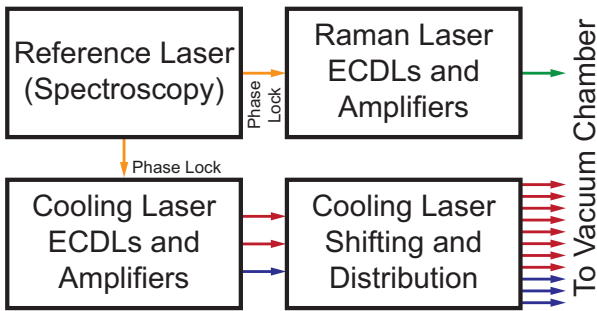


**Fig. 3** Modular concept of our laser system

range (FSR) of approximately 1.9 GHz. Control of the laser frequency is achieved by tuning of either the laser diode current or the cavity length (via a piezo). Applied separately, the mode-hop-free tuning range is limited to 200 MHz or the FSR of 1.9 GHz, respectively. However, by controlling both parameters simultaneously at a fixed gain ratio, a mode-hop free tuning range of about 9 GHz and thereby over more than the complete  $^{87}\text{Rb}$  D2 line was achieved (Figure 2).

To provide the various optical frequencies required to operate an atomic fountain interferometer and yet still maintain sufficient flexibility for future enhancements like quasi-continuous operation (many clouds of atoms in flight at the same time), a total of five ECDLs is employed. They are organized in four distinct modules: one reference laser module, two cooling laser modules and one Raman laser module (Figure 3).

The modules are mounted in a standard 19" electronics rack that has been fitted with inflatable air bags between its main body and its base plate which serve as a passive vibration isolation and also as a shock absorber for transport over rough terrain. A test transport over a snow-covered cobblestone surface has resulted in a decrease of fibre coupling efficiency of less than 30 percent. The rack is dimensioned such that it can fit through standard doors and is thereby easily transportable to different locations (Figure 4). For easy access, the laser modules are mounted on telescopic rails. The complete laser system and its control electronics could theoretically be mounted in just one rack – we chose, however, to also include other gravimeter electronics such as computer control, a backup power system, power supplies and diagnostic equipment which made a second rack necessary and enabled us to move mechanically noisy equipment (i.e. anything that includes cooling fans) away from the optics.

The dimensions of the complete system are  $177 \times 60 \times 60 \text{ cm}^3$  (computer and control electronics rack) plus  $194 \times 80 \times 60 \text{ cm}^3$  (laser rack), adding up to a total volume of  $1.6 \text{ m}^3$ . Power consumption is less than 1 kW.

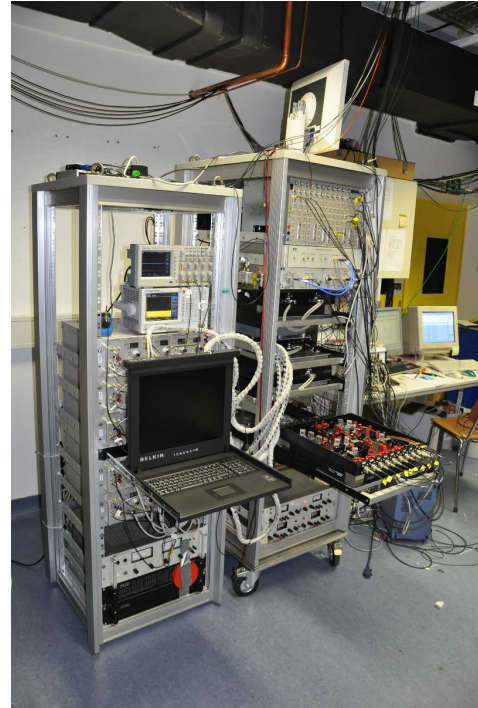


**Fig. 4** Photograph of laser system, cooling module 2 extended on telescopic rails. In addition to the complete laser system, these two racks also contain the gravimeter's computer, power supplies, emergency backup batteries, control electronics and diagnostic equipment

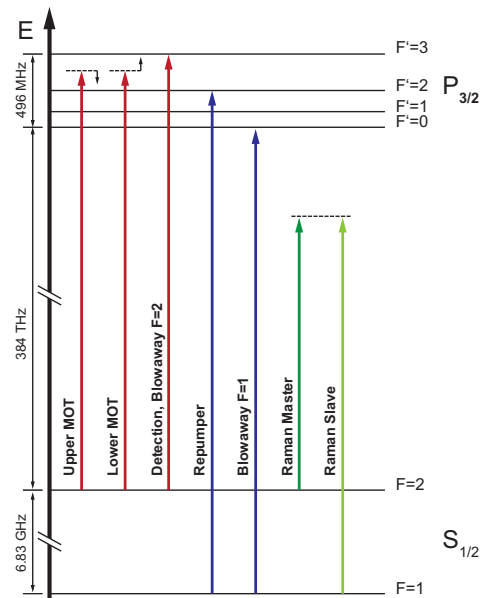


**Fig. 5**  $^{87}\text{Rb}$  D2 level scheme and laser frequencies required in our setup

### 3 Reference Laser

The reference laser module houses an ECDL that is stabilized 40 MHz below the  $^{85}\text{Rb}$   $F=3 \rightarrow F'=4$  transition by modulation transfer spectroscopy [20]. The control signal is used to stabilize the laser wavelength via the the laser diode's current controller. However, since this parameter is limited to a mode-hop free tuning range of 200 MHz, a second control path is employed: low-frequency components (below 100 Hz) of the control signal are applied to both the laser diode current as well as the piezo voltage at the fixed gain ratio determined to give us a mode-hop free tuning range of 9 GHz (see above). This way, slow drifts due to temperature variations or mechanical stress are compensated and the laser stays locked over days at its required frequency. In a laboratory test, the reference laser stayed locked even when slowly changing the module's temperature by 10 Kelvin over two hours. The reference laser is also impervious to moderately strong hits of a metallic wrench to its base plate. Comparing the system's open-loop and closed-loop frequency responses using a network analyzer, we measured a locking bandwidth of approximately 300 kHz (at 3dB below unity gain). This bandwidth is limited by electronics and cable lengths and not by the optical spectroscopy itself, as we reached a regime in which the atoms are pumped quickly into the desired internal states by using a pumping beam power of half a milliwatt with a beam diameter of one millimeter.

### 4 Cooling Laser System

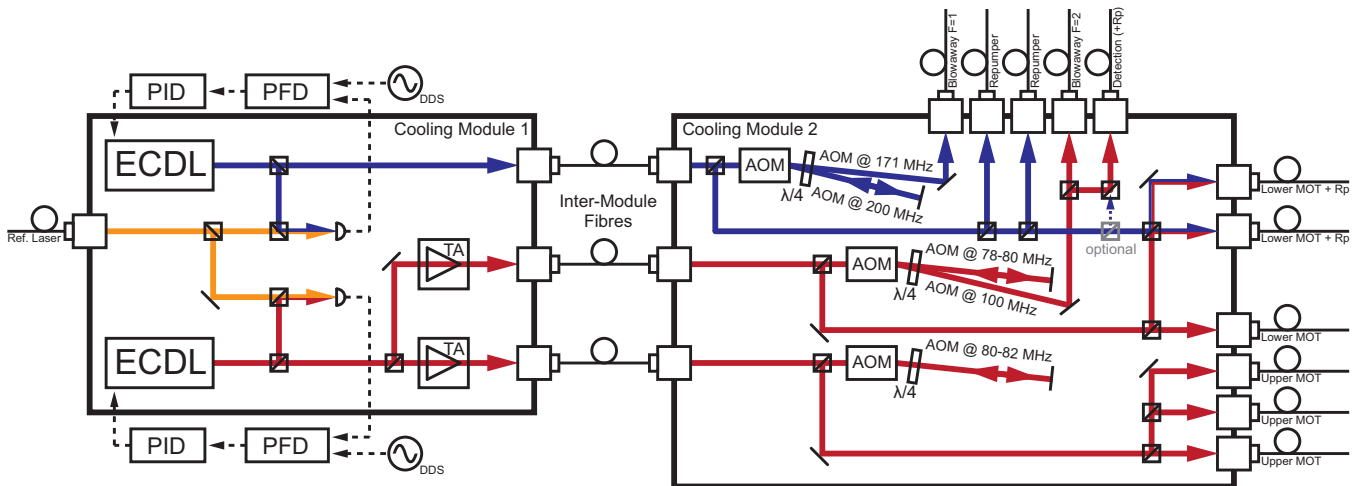
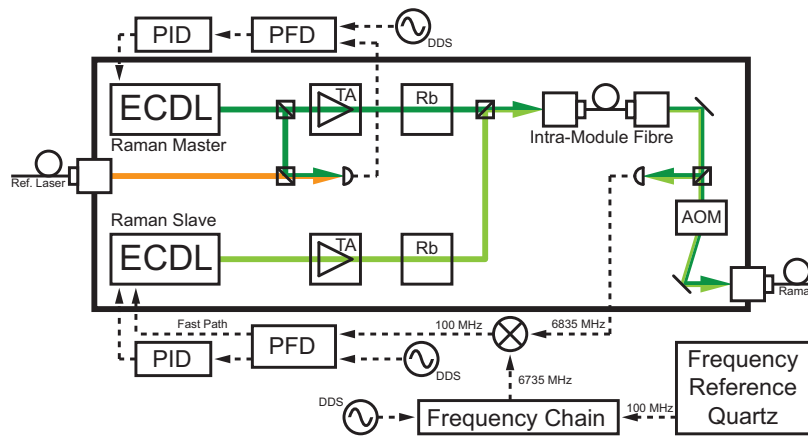
An atomic fountain setup requires a variety of optical frequencies in order to trap, cool, launch, select and detect the atoms, as can be seen in Figure 5. In our vacuum chamber, we capture the atoms in a Magneto-Optical Trap (MOT). Since the atom interferometer's sensitivity scales with the square root of both the repetition rate and the number of atoms, we aim to trap as many atoms as possible as quickly as possible. To achieve this, we use a large MOT volume (beam diameter 35 mm) at high laser power ( $> 300$  mW). In order to launch the atoms, both upper and lower MOT beams have to be detuned with respect to each other to achieve a moving molasses configuration [21]. Additionally, a repumper is required, as well as blow-away and detection light in both  $F=1 \rightarrow F'$  and  $F=2 \rightarrow F'$  frequency classes. A total of 11 separate fibre output ports at different laser powers and frequencies is required for full functionality.

Due to the large hyperfine ground splitting of 6835 MHz, light from the  $F=1 \rightarrow F'$  frequency class cannot easily (or with high efficiency) be shifted to  $F=2 \rightarrow F'$  by means of acousto-optical modulators. Hence, we employ two ECDLs mounted in the first cooling laser module, one for each frequency class. For frequency stabilization, light from each ECDL is overlapped with light from our

reference laser on a fast photodiode (Hamamatsu G4176-03) resulting in beat frequencies of about 5080 MHz and 1000 MHz, respectively. The signals frequencies are subsequently divided down to about 19.8 MHz (factor 256) and 100 MHz (factor 10), respectively. Comparing the resulting signal's zero-crossings to those of a stable Direct Digital Synthesizer (DDS) reference frequency in a Hittite HMC440QS16G digital phase-frequency detector (PFD) gives an error signal that we use to phase-lock the beat signal onto the DDS reference at a bandwidth of 200 kHz. This setup enables us to reach any desired laser frequency simply by changing the DDS frequency. The  $F=2 \rightarrow F'$  laser light is split into two halves of 12 mW each that are used to seed two Eagleyard tapered amplifiers (TPA-0780-01000), thereby amplifying laser power to two times one Watt. Both of these high-power beams mode-cleaned by an optical fiber at a coupling efficiency of only between 50 and 60 percent due to imperfections in the tapered amplifier's output laser beam profile. A third fibre is employed for the  $F=1 \rightarrow F'$  light (17 mW in-fibre).

In the second cooling laser module the light is frequency shifted and switched using acousto-optical modulators (AOMs), one for each of these three beams. This enables separate frequency and switching control of upper MOT, lower MOT and repumper beams. Not all eleven output ports will have to be used simultaneously, as for instance blow-away beams and MOT light are not required at the same time. By changing the AOMs' frequencies, the first order diffraction beam angle varies slightly. We make use of this effect and hit different mirrors at different AOM frequencies, one of which directs the light into one fibre, the other one reflects the light back into the AOM for a double pass configuration. Effectively, this enables us to switch between different fibre outputs at different laser frequencies within less than a microsecond without losing any light power at ports that are not in use at any given moment. Since the most light power is needed in the MOT phase of our experiment, the AOMs have been selected and adjusted so that they work at their center frequency and therefore peak efficiency of about 80 percent (single-pass) in that configuration. For producing blow-away and detection beams, less light power is sufficient, so we chose this configuration for driving the AOMs far detuned from their center frequency which resulted in single-pass efficiencies of 50 percent (driving an 80 MHz AOM at 100 MHz, Crystal Technology model 3080-125) and 60 percent (driving a 200 MHz AOM at 171 MHz, Crystal Technology model 3200-121).

To avoid unwanted scattered light, additional mechanical shutters (Sunex SHT934, switching time 1-2 ms) are used at each of the eleven output ports. We have not observed any influence of the shutters' mechanical noise on the fibre coupling efficiency. A schematic of this setup is shown in Figure 6, the total output power of this system in MOT configuration is six times 60 mW cool-


**Fig. 6** Layout of Cooling laser modules

**Fig. 7** Layout of Raman laser module

ing light plus 5 mW repumper light (in-fibre, coupling efficiency larger than 80 percent).

## 5 Raman Lasers

In order to induce an optical Raman transition between the hyperfine ground states of the atoms, a pair of two lasers with a fixed phase relation and a frequency difference of 6.835 GHz (the  $^{87}\text{Rb}$  ground state hyperfine splitting) is required to drive the two-photon transition via an intermediate level, as seen in Figure 5. In this section, we will describe our Raman laser system and its performance.

We employ two ECDLs (Figure 7) which emit light that is amplified to 1 Watt using tapered amplifiers and then overlapped. Rubidium vapour cells are employed to suppress unwanted amplified spontaneous emissions on atomic resonances. An AOM is used for fast switching and pulse-shaping of the Raman pulses. Identical pulse-shaping on both laser beams is ensured by an intra-module fibre common to both lasers where the light is mode-cleaned before entering the AOM. The Raman

master laser ECDL is phase-locked to the reference laser using a setup similar to the one employed in the cooling laser system, however the PFD we use here is an Analog Devices ADF4108.

The Raman slave laser ECDL is stabilised in frequency and phase in respect to the Raman master laser. Any phase noise between the two Raman lasers will be imprinted onto the atoms and will therefore directly limit the gravimeter's sensitivity. This is discussed in detail in section 6. Accordingly, the requirements in noise and locking bandwidth are much higher here than for the locks of the Raman master or the two cooling lasers. For this phase lock between the two ECDLs, light from both lasers is overlapped on a fast photodiode that is placed behind the intra-module fibre so that all noise sources that are not common to both beams (i.e. anything before overlapping and mode-cleaning done by the fibre) can be compensated for by the phase lock. The resulting beat signal of 6835 MHz is mixed down using a stable 6735 MHz reference. The resulting 100 MHz signal is phase-locked onto a DDS reference frequency using a Motorola MC100EP140 PFD. To overcome bandwidth limitations and thereby residual phase noise imposed by long cables



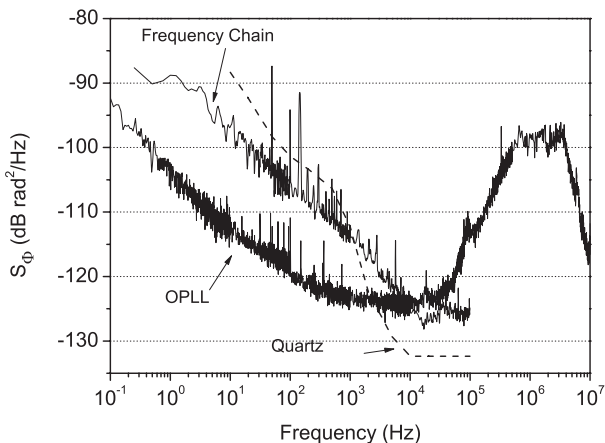


**Fig. 8** Phase noise spectral density for Raman laser OPLL, frequency chain (data from [11]) and quartz (DLR-100) at 6.8 GHz

and the laser diode current controller's response time, an additional high frequency control path is employed that modulates the ECDL laser diode's current directly via a small signal N-channel FET as a voltage to current converter and a lag-lead compensation network. Total cable lengths for this fast path add up to less than a meter.

The 6735 MHz mixing-down frequency is generated by a frequency chain that uses a Spectra Dynamics DLR-100 system as a frequency reference. The DLR-100 includes an ultra-low noise 100 MHz quartz that is locked to the 10th harmonic of a frequency-doubled 5 MHz quartz for even lower phase noise at low frequencies. The 100 MHz signal is multiplied to 6800 MHz and is then used to lock a Dielectric Resonator Oscillator (DRO) to 6735 MHz. This frequency chain is basically identical to the one described in [11].

By comparing the downconverted signal with the 100 MHz DDS reference using an independent mixer, we measured the phase noise spectral density of this optical phase lock loop (OPLL), see Figure 8. Between 100 Hz and 60 kHz, where our interferometer is most sensitive to noise (as shown in section 6), it largely stays below a level of -120 dB rad<sup>2</sup>/Hz (1  $\mu$ rad/Hz<sup>1/2</sup>). The achieved locking bandwidth is slightly above 4 MHz. However, since in this measurement any noise in either the frequency chain or the reference quartz is cancelled out, both of these noise sources have to be taken into account additionally in order to evaluate the performance of the complete system: Thus, Figure 8 also shows the phase noise spectral density of the frequency chain as described and characterized in [11] and that of the reference quartz system.

## 6 Gravimeter sensitivity

In this section, we will calculate the limit to our gravimeter's sensitivity due to phase noise from the Raman laser system. Of course, these are not the only noise sources

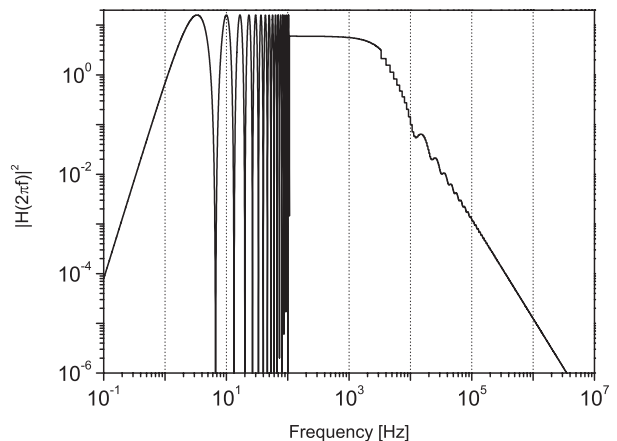


**Fig. 9**  $|H(2\pi f)|^2$  calculated for  $T=150$  ms and  $\tau=100$   $\mu$ s, averaged after 16 oscillations

in our gravimeter, as we are amongst others sensitive to mechanical vibrations and detection noise. These noise sources will be evaluated in future publications. In a setup like ours, the precision  $\frac{\Delta g}{g}$  with which we are able to measure local  $g$  in a single measurement is limited by the phase uncertainty  $\Delta\Phi$  as follows:

$$\frac{\Delta g}{g} = \frac{\Delta\Phi}{k_{\text{eff}} T^2 g} \quad (1)$$

The contribution of the Raman laser's power spectral density  $S_\Phi$  affects  $\Delta\Phi$  via a transfer, or weighting function,  $|H(\omega)|^2$ , i.e.  $\Delta\Phi$  can be evaluated as

$$\Delta\Phi^2 = \int_0^\infty |H(2\pi f)|^2 S_\Phi(f) df \quad (2)$$

In our setup we employ three Raman pulses: One  $\frac{\pi}{2}$ -pulse, one  $\pi$ -pulse, and finally another  $\frac{\pi}{2}$ -pulse. Assuming square Raman pulses of duration  $\tau$ , separated by time  $T$ , the explicit form for  $|H(\omega)|^2$  as derived in [22] is

$$|H(\omega)|^2 = \left| -\frac{4\Omega\omega}{\omega^2 - \Omega^2} \times \sin\left(\omega\frac{T+2\tau}{2}\right) \times \left[ \cos\left(\omega\frac{T+2\tau}{2}\right) + \frac{\Omega}{\omega} \times \sin\left(\omega\frac{T}{2}\right) \right] \right|^2 \quad (3)$$

with  $\Omega = \pi/2\tau_R$  being the Rabi oscillation frequency of the Raman transition. Due to a highly oscillatory behavior of  $H(\omega)$ , however, after the 16th oscillation only the average value is calculated (Figure 9) in order to avoid aliasing effects due to our limited data point spacing at higher frequencies. Also of note is the band pass filter behavior of  $|H(2\pi f)|^2$  whose effective lower cutoff frequency scales with  $T^{-1}$ , whereas the upper cutoff frequency scales with  $\tau^{-1}$ .

To evaluate the limit that our laser system imposes on gravimeter sensitivity, we calculate the root-mean-square of the spectra of the three contributing sources of phase noise in our system (OPLL, frequency chain, quartz) and multiply it with  $|H(2\pi f)|^2$ . Integrating over

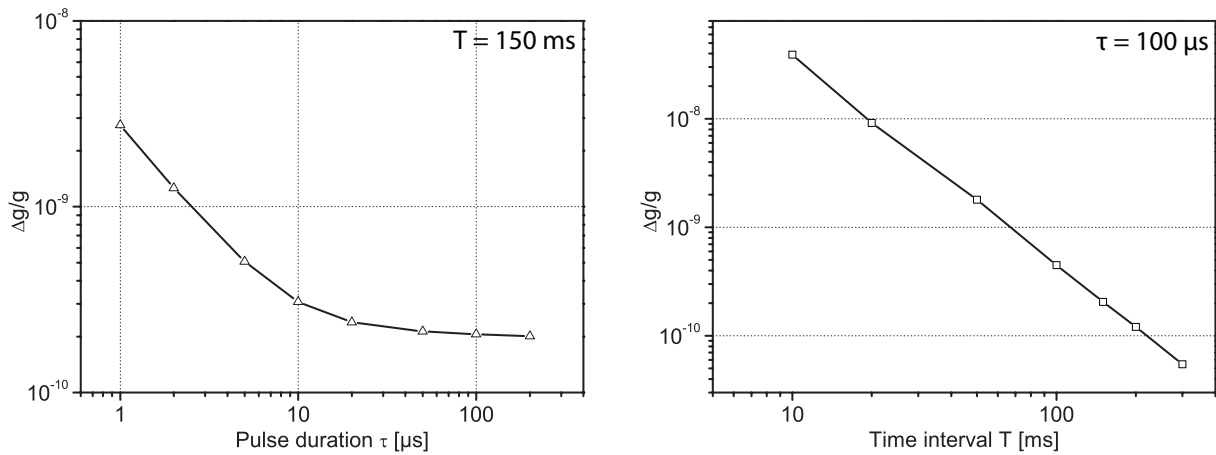


**Fig. 10** Sensitivity limit given by Raman laser phase noise for various values of  $\tau$  and  $T$

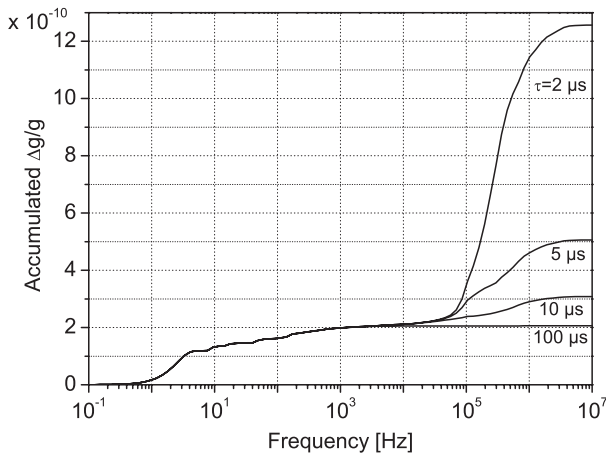


**Fig. 11**  $\Delta g/g$  as a function of the upper limit in the Raman laser power spectral density integration, displayed for various pulse lengths  $\tau$ .  $T = 150$  ms is held constant.

the complete frequency spectrum, we obtain our limits for  $\Delta\Phi^2$  and consequently for  $\frac{\Delta g}{g}$ . Assuming standard operating parameters for our gravimeter of  $T=150$  ms and  $\tau=100$   $\mu\text{s}$ , our single-shot sensitivity will be limited to  $\frac{\Delta g}{g} = 1.93 \times 10^{-10}$  by Raman laser phase noise.

For different  $T$  and  $\tau$ , the band pass behavior of the weighting function changes and so does our sensitivity to certain phase noise frequencies. The resulting sensitivity limits are shown in Figure 10. To illustrate which frequencies are the dominant contributors to these limit calculations, we have plotted an accumulation integral for different pulse lengths (Figure 11). In this diagram,  $\frac{\Delta g}{g}$  is plotted against  $x$  in  $\Delta\Phi^2 = \int_0^x |H(2\pi f)|^2 S_\Phi(f) df$ . As can be seen, our 4 MHz servo bump (see Figure 8) does not significantly contribute to the overall gravimeter sensitivity at long pulse lengths  $\tau$ , at shorter pulse lengths, however, the noise spectrum in the MHz range becomes a dominating factor. In contrast, a variation of pulse spacing  $T$  instead of  $\tau$  increases our sensitivity to low-frequency phase noise which is dominated by our quartz reference. This contribution is, however, not

nearly as significant as the fact that the sensitivity to  $g$  scales with  $T^{-2}$ , so we want to keep  $T$  as long as possible in our apparatus (see Figure 10).

## 7 Conclusion

We have designed and built a laser system for atom interferometry applications that is mobile and robust, yet still offers improvements over many conventional laboratory-based systems. This system enables us to operate a highly precise atom interferometer outside of standard laboratory conditions and thereby opens up new possibilities for geophysical gravity measurements.

## Acknowledgements

This work is supported by the European Commission (FINAQS, Contr. No. 012986-2 NEST), by ESA (SAI, Contr. No. 20578/07/NL/VJ) and by ESF/DFG (Euro-Quasar-IQS, DFG grant PE 904/2-1). We further thank LNE-SYRTE for design and construction of the frequency chain and the QUANTUS team for a fruitful collaboration.

## References

1. O. Carnal and J. Mlynek, *Phys. Rev. Lett.* **66**, 2689 (1991).
2. F. Riehle, T. Kisters, A. Witte, J. Helmcke and C. Borde, *Phys. Rev. Lett.* **67**, 177 (1991).
3. D. Keith, C. Ekstrom, Q. Turchette and D. Pritchard, *Phys. Rev. Lett.* **66**, 2693 (1991).
4. M. Kasevich and S. Chu, *Appl. Phys. B* **54**, 321 (1992).
5. H. Mueller, A. Peters and S. Chu, *Nature* **463**, 926 (2010).
6. S. Dimopoulos, P. W. Graham, J. M. Hogan and M. A. Kasevich, *Phys. Rev. D* **78**, p. 042003 (2008).
7. A. Peters, K. Chung and S. Chu, *Metrologia* **38**, 25 (2001).

8. T. Gustavson, A. Landragin and M. Kasevich, *Class. Quantum Grav.* **17**, 2385 (2000).
9. M. Snadden, J. McGuirk, P. Bouyer, K. Haritos and M. Kasevich, *Phys. Rev. Lett.* **81**, 971 (1998).
10. M. de Angelis, A. Bertoldi, L. Cacciapuoti, A. Giorgini, G. Lamporesi, M. Prevedelli, G. Saccorotti, F. Sorrentino and G. M. Tino, *Meas. Sci. Technol.* **20**, p. 022001 (2009).
11. J. Le Gouet, T. E. Mehlstaebler, J. Kim, S. Merlet, A. Clairon, A. Landragin and F. P. Dos Santos, *Appl. Phys. B* **92**, 133 (2008).
12. G. Stern, B. Battelier, R. Geiger, G. Varoquaux, A. Villing, F. Moron, O. Carraz, N. Zahzam, Y. Bidet, W. Chaibi, F. P. Dos Santos, A. Bresson, A. Landragin and P. Bouyer, *Eur. Phys. J. D* **53**, 353 (2009).
13. P. Cheinet, F. Pereira Dos Santos, T. Petelski, J. Le Gouet, J. Kim, K. T. Therkildsen, A. Clairon and A. Landragin, *Appl. Phys. B* **84**, 643 (2006).
14. G. M. Tino, L. Cacciapuoti, K. Bongs, C. J. Borde, P. Bouyer, H. Dittus, W. Ertmer, A. Goerlitz, M. Inguscio, A. Landragin, P. Lemonde, C. Lammerzahl, A. Peters, E. Rasel, J. Reichel, C. Salomon, S. Schiller, W. Schleich, K. Sengstock, U. Sterr and M. Wilkens, *Nucl. Phys. B.* **166**, 159 (2007).
15. S. G. Turyshev, U. E. Israelsson, M. Shao, N. Yu, A. Kuzenko, E. L. Wright, C. W. F. Everitt, M. Kasevich, J. A. Lipa, J. C. Mester, R. D. Reasenber, R. L. Walsworth, N. Ashby, H. Gould and H. J. Paik, *Int. J. Mod. Phys. D* **16**, 1879 (2007).
16. B. Dubetsky and M. A. Kasevich, *Phys. Rev. A* **74**, p. 023615 (2006).
17. L. Timmen, O. Gitlein, J. Mueller, G. Strykowski and R. Forsberg, *Zeitschrift fuer Vermessungswesen* **133/3**, 149 (2008).
18. T. van Zoest, N. Gaaloul, Y. Singh, H. Ahlers, W. Herr, S. T. Seidel, W. Ertmer, E. Rasel, M. Eckart, E. Kajari, S. Arnold, G. Nandi, W. P. Schleich, R. Walser, A. Vogel, K. Sengstock, K. Bongs, W. Lewoczko-Adamczyk, M. Schiemangk, T. Schuldt, A. Peters, T. Koenemann, H. Muentinga, C. Laemmerzahl, H. Dittus, T. Steinmetz, T. W. Haensch and J. Reichel, *Science* **328**, 1540 (2010).
19. X. Baillard, A. Gauguet, S. Bize, P. Lemonde, P. Laurent, A. Clairon and P. Rosenbusch, *Opt. Comm.* **266**, 609 (2006).
20. J. Supplee, E. Whittaker and W. Lenth, *Appl. Opt.* **33**, 6294 (1994).
21. M. Kasevich, D. Weiss, E. Riis, K. Moler, S. Kasapi and S. Chu, *Phys. Rev. Lett.* **66**, 2297 (1991).
22. P. Cheinet, B. Canuel, F. P. Dos Santos, A. Gauguet, F. Yver-Leduc and A. Landragin, *IEEE Trans. Instrum. Meas.* **57**, 1141 (2008).